Properties of $Bi_2Sr_2CaCu_2O_8$ thick films melt-processed at temperatures up to 950 °C

W. C. McGinnis and J. S. Briggs
Naval Ocean Systems Center, Code 573, San Diego, California 92152-5000

(Received 17 June 1991; accepted 5 November 1991)

Thick $Bi_2Sr_2CaCu_2O_8$ films have been produced by melting $Bi_2Sr_2CaCu_2O_8$ powder on MgO substrates at temperatures just above the melting temperature of the powder. X-ray diffraction measurements indicate enhanced c-axis alignment throughout the thickness of the films. Films melted at 900 °C show greater alignment and contain less $Bi_2Sr_2CuO_6$ compared to those processed at 950 °C. Both the degree of alignment and the $Bi_2Sr_2CuO_6$ content increase as the cooling rate is decreased. Transport measurements show that films quickly cooled from low melt-processing temperatures have the highest critical current densities (J_c = 13 kA/cm^2 at 30 K). The temperature dependence of J_c is best described by a flux creep model. Finally, J_c at 4.2 K (in both parallel and perpendicular magnetic fields) undergoes a sudden drop at low fields, but levels off above 0.5 T to about 30% of the zero field value.

I. INTRODUCTION

Numerous research groups have investigated melt-processing or texturizing techniques[1–6] as a way of improving the critical current density J_c of high transition temperature superconductors such as $YBa_2Cu_3O_7$ and $Bi_2Sr_2CaCu_2O_8$. J_c is maximized in these highly anisotropic materials by aligning the individual single-crystal grains with each other so that current flows parallel to the copper-oxygen planes. The crystal unit cell is typically orthorhombic, with a c-axis spacing 2 to 7 times that of an approximately equal a-axis and b-axis spacing. These elongated unit cells bond to form flat platelets whose flat surface is parallel to the a-b (copper-oxygen) planes. The platelet-like crystals, given the opportunity, will lie flat against each other. Reasonably good alignment can be produced by simply pressing the powder. Such alignment has been observed by x-ray diffraction measurements of pressed pellets[7] and even of powder that has been finger-pressed on a microscope slide. C-axis alignment has also been enhanced by using a strong magnetic field to align the magnetic rare-earth ions (R) in $RBa_2Cu_3O_7$ samples.[8] An even more effective alignment technique is to melt the material and then let it solidify. The degree of alignment will depend on the cooling rate and other conditions.

Although melt-processing produces highly oriented samples, it can have the possible drawback of changing the phase makeup of the sample. The high T_c ceramic superconducting compounds contain four, five, or more elements which can be redistributed into a number of other compounds upon solidification from the melt of the parent compound. For example, the Bi–Sr–Ca–Cu–O family of superconductors includes phases with the nominal compositions $Bi_2Sr_2CuO_6$, $Bi_2Sr_2CaCu_2O_8$, and $Bi_2Sr_2Ca_2Cu_3O_{10}$.[9] In addition, nonsuperconducting compounds such as cuprates of Ca and Sr can form. The superconducting properties of the sample are generally degraded by the presence of these unwanted phases and compounds (although very finely dispersed impurities or defects can increase flux pinning and give higher J_c[10,11]). It can be important, therefore, to maintain the phase purity of melted samples while achieving alignment of the superconducting planes.

This paper compares the phase makeup, crystalline alignment, surface morphology, and superconducting properties of thick $Bi_2Sr_2CaCu_2O_8$ films melt-processed at about 10 to 15 °C above the melting temperature (approximately 885 °C) of $Bi_2Sr_2CaCu_2O_8$ with those of films melted at about 65 °C above that temperature. These properties are also studied as a function of cooling rate (from a few °C/s to a few °C/h). The phase purity and crystalline alignment of the samples are characterized by x-ray diffraction, while the surface morphology is studied by scanning electron microscopy. Resistance versus temperature measurements and transport critical current density as a function of temperature and magnetic field are also reported.

II. EXPERIMENTAL PROCEDURES

Prior to making the thick films, $Bi_2Sr_2CaCu_2O_8$ powder was prepared by solid state reaction nominally as follows. Stoichiometric amounts of Bi_2O_3, $SrCO_3$, $CaCO_3$, and CuO powders, all at least 99.999% pure, were mixed and ground together. The mixture was calcined at 840 °C for 36 h. The material was then reground and processed at 848 °C for 40 h. All processing was done in air. The powder used for the thick films was obtained by grinding the resulting material. Pellets pressed

from this powder and sintered at 850 °C for 20 h in air had a zero resistance transition temperature of 78 K. X-ray diffraction measurements showed no indication of the $Bi_2Sr_2CuO_6$ or $Bi_2Sr_2Ca_2Cu_3O_{10}$ superconducting phases.

Several candidate substrate materials were used to make melt-processed films at 950 °C, including polycrystalline Al_2O_3 and single crystals of MgO, yttria-stabilized ZrO_2, and Si. The $Bi_2Sr_2CaCu_2O_8$ compound showed substantial reaction with Al_2O_3 and very strong reaction with Si. No visible reaction was observed with the other two substrate materials, and both produced films with sharp superconducting transitions at about 80 K. The best films were obtained using the MgO substrates, however, because the films did not adhere well to the ZrO_2 substrates. Therefore, MgO was chosen as the substrate material for this study. All of the films described below were melted on single crystal substrates of (100)-oriented, polished MgO.

The $Bi_2Sr_2CaCu_2O_8$ powder described above was thoroughly ground and mixed with a small amount of liquid (either methanol or polyglycol) to form a spreadable paste. The mixture was spread evenly over a substrate with a razor blade or by screen-printing. The thickness of this coating determined the ultimate film thickness. The samples were placed in a furnace, heated from room temperature to 200 °C, and held there for 1 h to remove the carrier liquid. The temperature was then increased at 5 °C/min to the melt-processing temperature T_{melt}, and held at that temperature for 30 min to melt the $Bi_2Sr_2CaCu_2O_8$ powder. The films were cooled to 850 °C at a given cooling rate, held there for 6 h, and cooled at 5 °C/min to room temperature. All processing was done with the samples in air.

All films were characterized by x-ray diffraction, using a Rigaku RU-200B diffractometer with Cu K_α radiation, and by 4-probe resistance versus temperature measurements, using a closed-cycle refrigerator. Some films were scribed in a block "S" pattern for critical current density measurements. A 2 mm wide by 4 mm long low-critical-current section (the middle part of the "S") was formed by scribing two 7 mm long lines from opposite sides of the 10 mm × 10 mm substrate, with a separation distance of 2 mm. The maximum self-field per unit of current for this configuration is estimated to be 0.4 mT/A. Low resistance contacts were made to the other (high-critical-current) sections of the film by heating silver paint pads at 800 °C in air for 2 h, and then indium-soldering wires to the pads. The current-voltage characteristics were obtained using a previously described pulsed-current technique.[12]

A series of films (using polyglycol as a carrier liquid) were melted at 900 °C and cooled at rates of 240 °C/min (step-cooled from T_{melt}), 1 °C/min, and 0.1 °C/min. After scribing for J_c measurements, these films had weak-link cross sections of 0.29, 0.34, and 0.12 mm^2, respectively (with corresponding film thicknesses of 146, 179, and 131 μm). For comparison, other films were processed in the same way but with T_{melt} = 950 °C. Of these latter films, only the step-cooled sample produced a reasonably smooth, uniform-looking film, and therefore only that film was characterized. The weak-link cross section of this 231 μm thick film after scribing was 0.38 mm^2.

In order to compare the properties of a film with the as-melted surface intact and with it removed, a 390 μm thick film with T_{melt} = 895 °C (methanol carrier liquid, cooling rate = 1 °C/min) was thinned down to a thickness of 154 μm using fine grinding paper. J_c in zero applied magnetic field was measured at various temperatures in the closed-cycle refrigerator both before and after thinning the film. The critical current was determined with a 10 μV/cm electric field criterion. The cross-sectional area of the weak link was 0.82 mm^2 for the as-melted film and 0.32 mm^2 for the thinned film. J_c (4.2 K) was measured again, with the thinned film immersed in liquid helium, in magnetic fields up to 8 T, both with the film perpendicular and parallel to the field. For each field orientation, the current flow was perpendicular to the field. The data were collected in ever increasing magnetic fields to avoid trapped flux or hysteresis effects.

III. RESULTS AND DISCUSSION

The x-ray diffraction spectrum for one of the films melted at 900 °C is shown in Fig. 1. Nearly all of the peaks are identified as (00*lm*) peaks, with $l + m = 2n$, indicating fairly strong c-axis alignment. The $m = 0$ peaks are main reflections, while the $m = \pm 1$ peaks are due to first-order satellite reflections[13] resulting from the modulated structure[14] of this compound. Note that the intensity is plotted on a square root scale in order to bring out the low intensity peaks. All of the films melted at 900 °C or below show similar c-axis alignment, varying somewhat with cooling rate. The relative degree of alignment and its dependence on cooling rate is indicated by the x-ray rocking curve results listed in Table I. Blank entries in the table indicate the lack of a well-defined rocking curve peak.

Films melted at 950 °C, as well as some of those melted at 900 °C, contain both the $Bi_2Sr_2CaCu_2O_8$ and $Bi_2Sr_2CuO_6$ phases. An indication of the relative amount of the two phases in the 900 °C-melted films is presented in Fig. 2, which shows the (0020) peak region. Only for the film step-cooled from 900 °C is $Bi_2Sr_2CuO_6$ undetected in the x-ray spectrum.

The surface of the film melted at 895 °C had a shiny, glass-like appearance. However, it was not known if the c-axis alignment observed in diffraction measurements

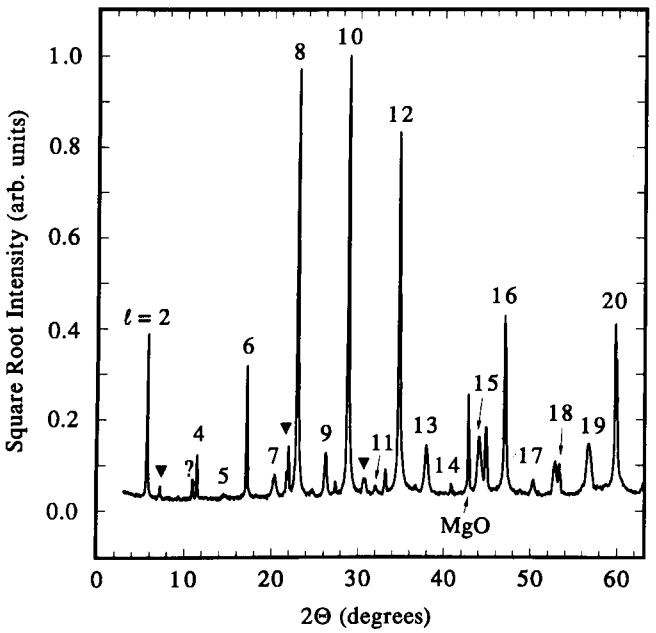

FIG. 1. X-ray diffraction spectrum of $Bi_2Sr_2CaCu_2O_8$ film melted at 900 °C and cooled at 0.1 °C/min. The peak intensity is plotted on a square root scale. $Bi_2Sr_2CaCu_2O_8$ (00*lm*) peaks are labeled with the value of *l*. Even values are main reflections ($m = 0$), while odd values are satellite reflections ($m = \pm 1$). Possible $Bi_2Sr_2CuO_6$ peaks and unidentified peaks are marked by inverted triangles and question marks, respectively.

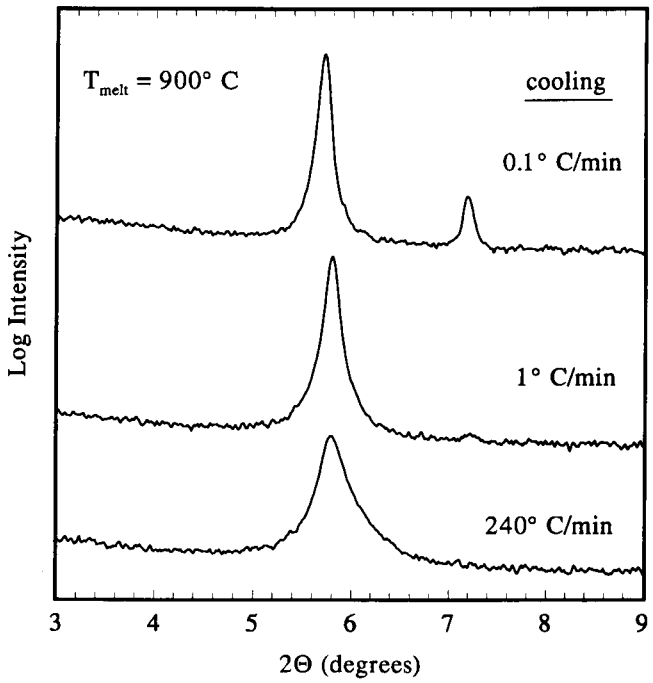

FIG. 2. X-ray diffraction spectra in the low-angle region for films melted at 900 °C with various subsequent cooling rates. The (0020) peaks of the $Bi_2Sr_2CaCu_2O_8$ phase are at about 5.7°, and those of the $Bi_2Sr_2CuO_6$ phase are at about 7.2°.

was localized to the surface layer or if it extended throughout the bulk of the film. To answer this question, the surface was removed as described above and another diffraction spectrum obtained. This spectrum is shown on a linear intensity scale in Fig. 3 for mid-range values of 2θ, along with the spectrum of $Bi_2Sr_2CaCu_2O_8$ powder from the batch used to make the film. The relative intensities of the spectra have been adjusted so that the non-(00*lm*) peaks are approximately equal in height. Although the c-axis alignment is not as complete as in the as-melted film (with x-ray spectrum similar to that in Fig. 1), the (0080), (00 $\underline{1}$0 0), and (00 $\underline{1}$2 0) peaks still show significant enhancement compared to other peaks.

The resistance versus temperature characteristics typical of these films are shown in Fig. 4. Because the

TABLE I. Full width half maximum (FWHM) of rocking curves taken about the (0060) and (0080) peaks of the 900 °C-melted films and of the starting $Bi_2Sr_2CaCu_2O_8$ powder.

Sample	FWHM about (0060)	FWHM about (0080)
0.1 °C/min film	3.91°	...
1 °C/min film	5.52°	5.82°
240 °C/min film	6.80°	7.84°
Starting powder	...	9.86°

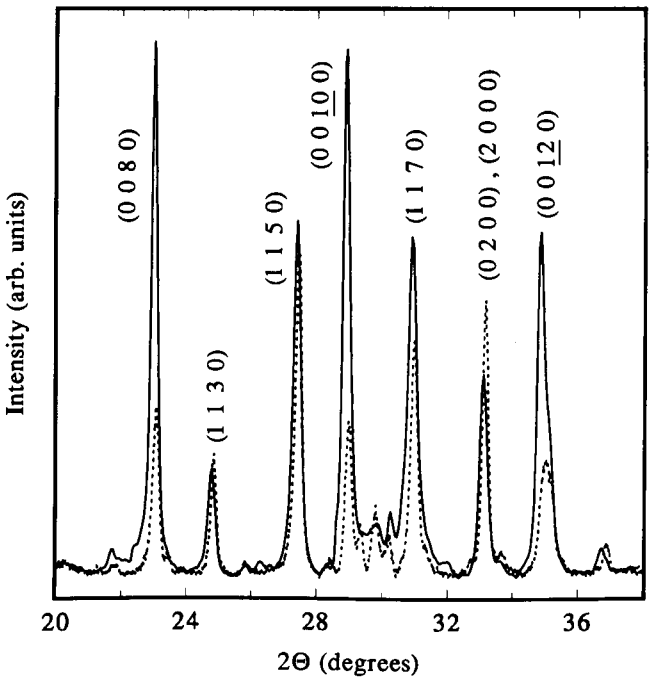

FIG. 3. X-ray diffraction spectra of 895 °C-melted $Bi_2Sr_2CaCu_2O_8$ film after being thinned with fine grinding paper (solid line) and of $Bi_2Sr_2CaCu_2O_8$ starting powder (dashed line). The main peaks are labeled by their Miller indices. The relative intensities of the spectra have been adjusted so that the non-(00*lm*) peaks are approximately equal in height.

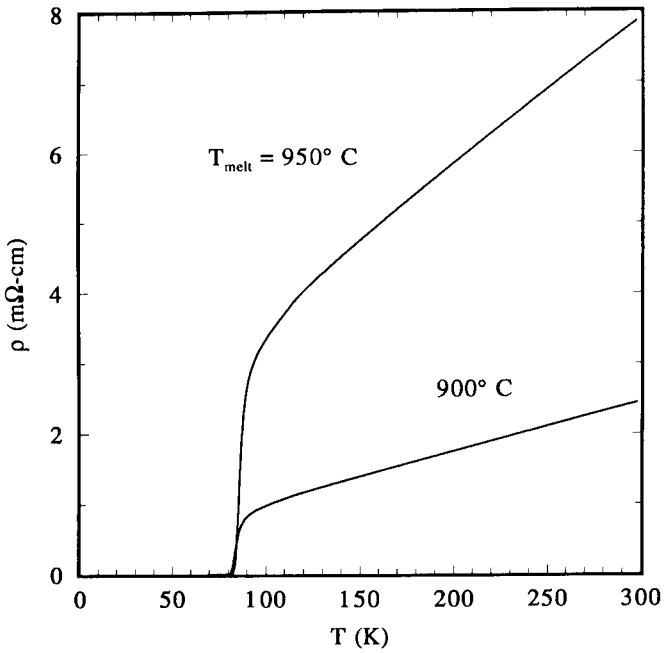

FIG. 4. Resistivity versus temperature of $Bi_2Sr_2CaCu_2O_8$ films melted at the temperatures shown and then step-cooled to the annealing temperature of 850 °C.

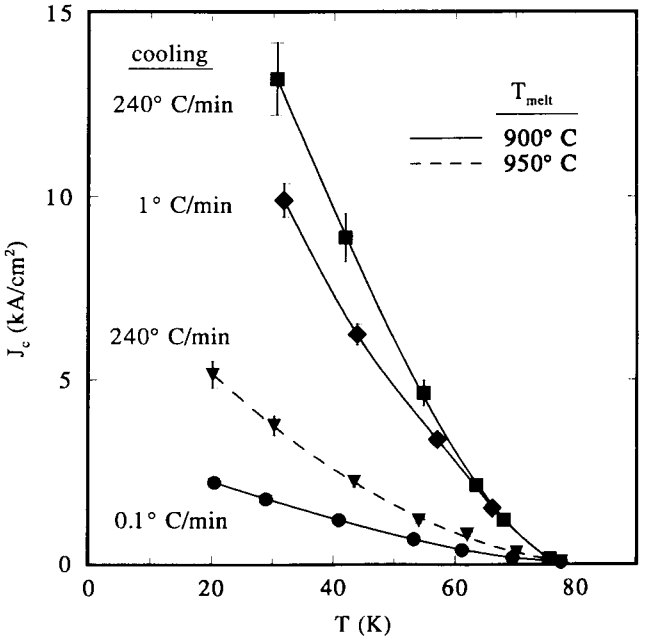

FIG. 5. Transport critical current density versus temperature in zero applied magnetic field for $Bi_2Sr_2CaCu_2O_8$ films with the cooling rates shown. The lines are guides to the eye for films melted at 900 °C (solid lines) and 950 °C (dashed line).

processing was done in air, the zero-resistance transition temperatures are in the range of 80 to 83 K. By reducing the oxygen pressure during the annealing step at 850 °C and subsequent cooling to room temperature, the value of T_c could have been increased to above 90 K.[15,16] The resistivity curve of the 900 °C, step-cooled film shown in the figure is typical of the films melted at the same temperature but cooled more slowly.

Figure 5 illustrates the variation of J_c with melting temperature and cooling rate, as well as the temperature dependence. The highest J_c is obtained for films melted at 900 °C, rather than 950 °C, as seen by comparing the two step-cooled films. This result is consistent with the smaller degree of c-axis alignment for the 950 °C film, as evidenced by the lack of *(00lm)* peak enhancement in its x-ray diffraction spectrum, as well as with the much rougher surface morphology, as seen in Fig. 6. The differences in morphology might also explain the resistivity characteristics seen in Fig. 4. Comparison of the three films melted at 900 °C in Fig. 5 clearly shows that the best J_c values are obtained for the more quickly cooled films. This, however, is not the result expected based on c-axis alignment considerations (see Table I). Nor is this dependence easily understood in terms of the morphology. Although it may not be clear from Fig. 6, the slower the cooling rate for the 900 °C films, the larger the crystalline features of the film. A comparison of Figs. 2 and 5, however, indicates that the films with higher J_c values are those with less of the $Bi_2Sr_2CuO_6$ phase.

The temperature dependence of J_c in zero applied field is plotted in Fig. 7 for the thinned 895 °C film. The solid line is a least-square fit of the data to an expression for the critical current density based on the flux-creep model (using the notation of Savvides[17]):

$$\frac{c}{s} = \exp\left[\frac{-u_0(1+t^2)(1-t^2)}{t}\right]\sinh\left(\frac{s^{1/2}}{t}\right) \quad (1)$$

where $t = T/T_c$ is the reduced temperature, $u_0 kT_c$ is the zero temperature pinning energy, and the dimensionless parameters c and s are given by:

$$c = \frac{E_c\Phi_0^3}{v_0}\left(\frac{a_p}{\beta kT_c}\right)^2$$
$$s(t) = \frac{J(t)\Phi_0^3}{\beta}\left(\frac{a_p}{kT_c}\right)^2. \quad (2)$$

Here E_c is the electric field criterion defining the critical current, a_p is the distance between pinning sites, the self-field is proportional to the current density and is given by βJ_c, v_0 is the flux line drift velocity in the absence of pinning, Φ_0 is the flux quantum, and k is Boltzmann's constant. Note that s and J_c are related by $J_c(t)/J_c(0) = s(t)/s(0)$. The sinh (Lorentz force) term of Eq. (1) assumes a force per unit length of $J_c\Phi_0$ acting on a flux line (or bundle of flux lines) of length a_p over a hop distance equal to the flux line lattice spacing a_0 (or na_0 for a bundle of n flux lines). The exponential (pinning) term of Eq. (1) is based on a pinning energy

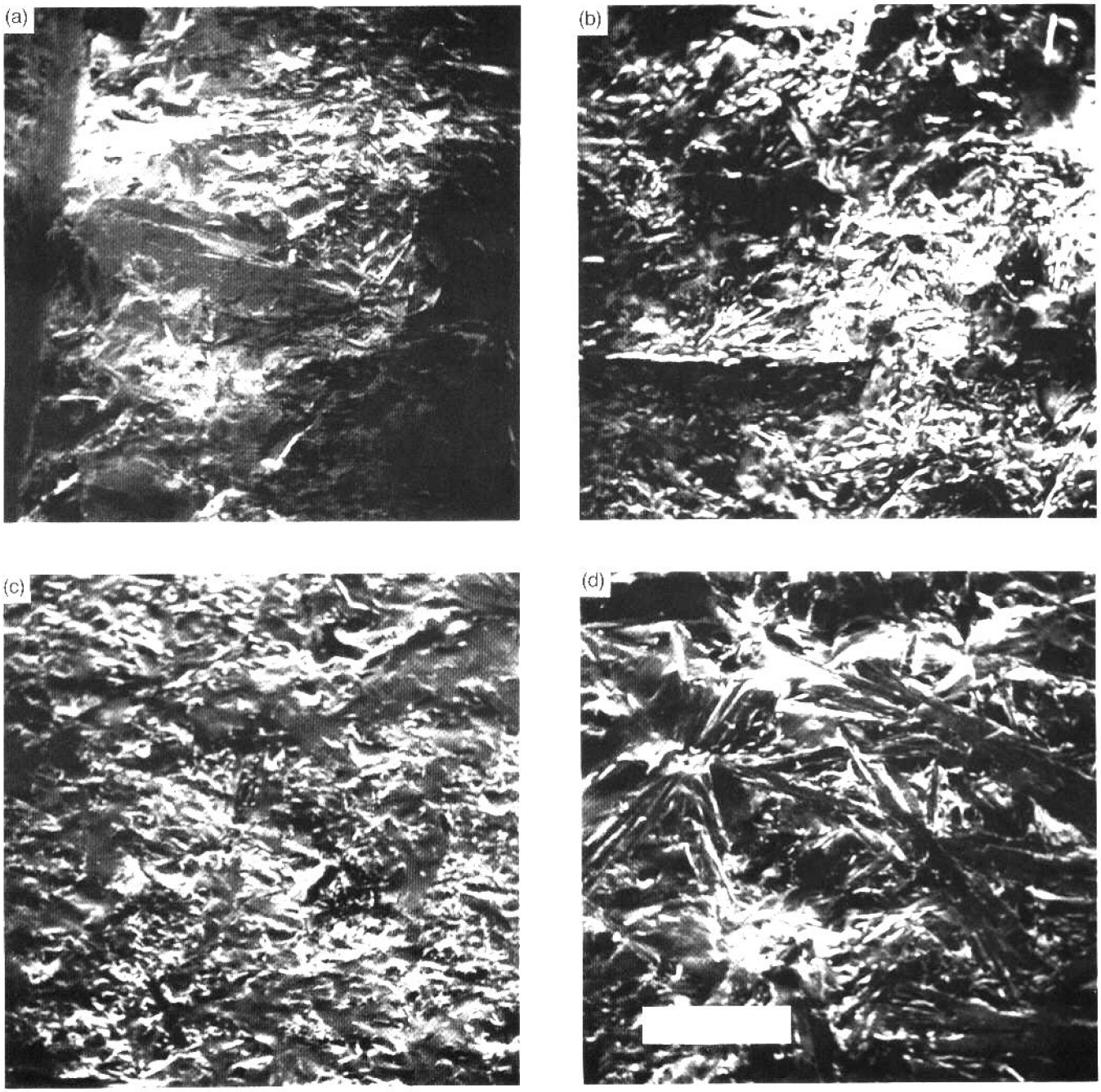

FIG. 6. Scanning electron micrographs for the 900 °C-melted $Bi_2Sr_2CaCu_2O_8$ films cooled at (a) 0.1 °C/min, (b) 1 °C/min, and (c) 240 °C/min, and for the (d) 950 °C-melted film cooled at 240 °C/min. The magnification, indicated by the 300 μm long white bar in (d), is the same for all four films. A vertical scribe line can be seen on the far left side of (a).

$U \sim H_c^2 \xi^2 D$, where $H_c(t)$ is the thermodynamic critical magnetic field, $\xi(t)$ is the Ginsberg–Landau coherence length, and D is the diameter of a pinning center (grain boundaries, voids, etc.). All of the films characterized here show this flux-creep temperature dependence of J_c. In fact, when the J_c values of all five films of Fig. 5 are normalized to the respective values at 30 K, all of the data falls on a common curve. Fitting the data to weak-link models (assuming either superconductor/insulator/superconductor or superconductor/normal-metal/superconductor junctions at the grain boundaries) gives unsatisfactory results.

The magnetic field dependence of the critical current density of the thinned 895 °C film is shown in Fig. 8. Measurements were performed both with the field parallel and perpendicular to the film. Both curves are

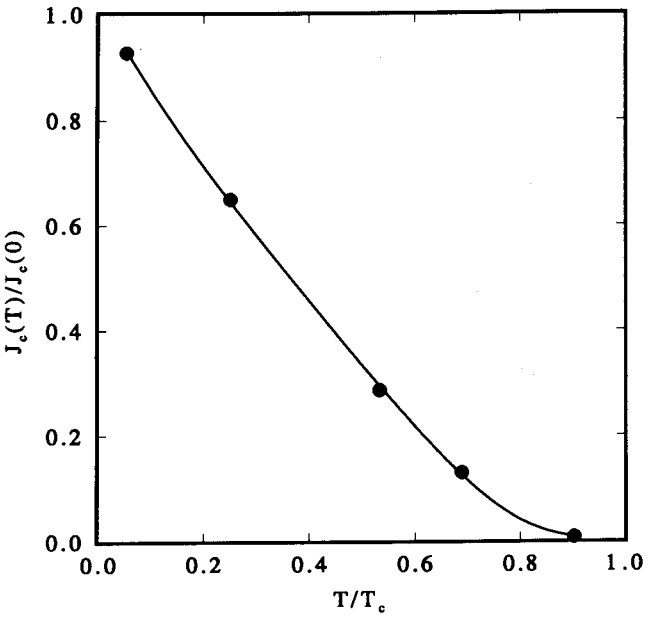

FIG. 7. Temperature dependence of the normalized critical current density in zero applied magnetic field for the 895 °C-melted $Bi_2Sr_2CaCu_2O_8$ film after thinning. The solid line is a least-square fit to Eq. (1) with $c = 0.0185$, $u_0 = 9.02$, and $s(0) = 79.8$. The critical current density at zero temperature is 8941 A/cm^2 and the zero-resistance critical temperature is 79 K.

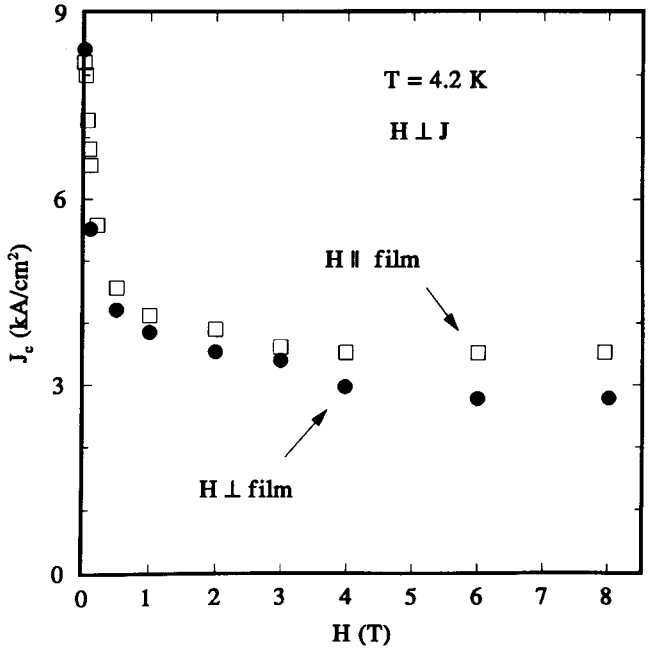

FIG. 8. Transport critical current density versus magnetic field, both parallel and perpendicular to the film, of the 895 °C-melted $Bi_2Sr_2CaCu_2O_8$ film after thinning. The current flow was perpendicular to the magnetic field in both cases.

characterized by J_c undergoing a rapid drop in the low magnetic field region, and then leveling off at fields above 0.5 T or so. The initial decrease in J_c might be attributed to the strong magnetic field dependence of the tunneling current of Josephson junctions formed between weakly linked superconducting grains.[18,19] As pointed out by Dew-Hughes, however, J_c should continue to fall toward zero with increasing field.[20] A possible explanation[21] is that at zero field, the current in these thick films is carried by a parallel combination of high-J_c superconducting material with no weak links (carrying a maximum current I_0 through an area A_0) and high-J_c material connected by weak links (carrying a maximum current I_w through an area A_w). The measured critical current density J_c is then the sum of the critical currents divided by the total area, or $(I_0 + I_w)/(A_0 + A_w)$. As a magnetic field is applied, the tunneling critical current I_w falls off rapidly while I_0 decreases more gradually. If the zero field values of I_w and I_0 are comparable, then the field dependence shown in the figure is expected. Similar arguments can be made assuming a distribution of grain-to-grain links with strengths ranging from strong to weak.[22] Such an assembly of grain-to-grain links might consist of a combination of anisotropy-limited[23] (due to relative misorientation of adjacent grains) links and Josephson-junction-limited[24] (due to normal or insulating barriers between grains) links.

In contrast to the highly anisotropic critical current densities measured in single crystals of $Bi_2Sr_2CaCu_2O_8$ ($J_{c\parallel}/J_{c\perp} \approx 10^3$, where $\parallel$ refers to current in the a-b plane),[25] the J_c values shown in Fig. 8 are only weakly dependent on the orientation of the magnetic field with respect to the film surface (and therefore presumably with respect to the c-axis of these partially aligned films). This observation is consistent with the presence of at least some weak links between grains. As suggested by Hampshire *et al.*,[26] the weak-linked granular nature of the material causes the current to follow a tortuous path among the grains, and so, on the granular scale, the direction of the current with respect to the magnetic field is not constant.

IV. SUMMARY

The crystalline and superconducting properties of melt-processed $Bi_2Sr_2CaCu_2O_8$ thick films have been investigated as a function of melt temperature (895 °C to 950 °C) and cooling rate (0.1 °C/min to 240 °C/min) from the melt-processing temperature to the anneal temperature of 850 °C. X-ray diffraction measurements indicate that the $Bi_2Sr_2CuO_6$ content increases as the cooling rate is decreased and as the melt temperature is increased. Also from the x-ray data, c-axis alignment increases as the cooling rate is decreased, but decreases with increasing melt temperature. The highest critical currents were obtained for films step-cooled from the lower melt temperatures (900 °C). These films also had the lowest $Bi_2Sr_2CuO_6$ content. All films, however, showed the

same functional dependence, best described by flux-creep models, of J_c on temperature. The sharp initial decrease and subsequent leveling-off of J_c with magnetic field can be understood in terms of the coexistence of strong and weak links between single-crystal grains.

ACKNOWLEDGMENT

This work was supported by the Independent Exploratory Development Program at the Naval Ocean Systems Center.

REFERENCES

1. S. Jin, T. H. Tiefel, R. C. Sherwood, R. B. van Dover, M. E. Davis, G. W. Kammlott, and R. A. Fastnacht, Phys. Rev. B **37**, 7850 (1988).
2. K. Salama, V. Selvamanickam, L. Gao, and K. Sun, Appl. Phys. Lett. **54**, 2352 (1989).
3. H. W. Neumüller and G. Ries, Physica C **162-164**, 363 (1989).
4. M. Peuckert, W. Becker, J. Bock, B. Hettich, H.-W. Neumüller, and M. Schwarz, Physica C **162-164**, 893 (1989).
5. W. Zhu, M. M. Miller, P. A. Metcalf, C. S. Calhoun, and H. Sato, Mater. Lett. **7**, 247 (1988).
6. J. R. Spann, L. E. Toth, I. K. Lloyd, M. Kahn, M. Chase, B. N. Das, T. L. Francavilla, and M. S. Osofsky, J. Mater. Res. **5**, 1163 (1990).
7. J. Huang, T. Li, X. Xie, J. Zhang, T. Chen, and T. Wu, Mater. Lett. **6**, 222 (1988).
8. D. E. Farrell, B. S. Chandrasekhar, M. R. DeGuire, M. M. Fang, V. G. Kogan, J. R. Clem, and D. K. Finnemore, Phys. Rev. B **36**, 4025 (1987).
9. J. M. Tarascon, W. R. McKinnon, P. Barboux, D. M. Hwang, B. G. Bagley, L. H. Greene, G. W. Hull, Y. LePage, N. Stoffel, and M. Giroud, Phys. Rev. B **38**, 8885 (1988).
10. M. Murakami, M. Morita, K. Doi, and K. Miyamoto, Jpn. J. Appl. Phys. **28**, 1189 (1989).
11. A. Umezawa, G. W. Crabtree, J. Z. Liu, H. W. Weber, W. K. Kwok, L. H. Nunez, T. J. Moran, C. H. Sowers, and H. Claus, Phys. Rev. B **36**, 7151 (1987).
12. W. C. McGinnis, E. W. Jacobs, C. D. Rees, and T. E. Jones, Rev. Sci. Instrum. **61**, 984 (1990).
13. M. Onoda, A. Yamamoto, E. Takayama-Muromachi, and S. Takekawa, Jpn. J. Appl. Phys. **27**, L833 (1988).
14. G. Calestani, C. Rizzoli, M. G. Francesconi, and G. D. Andreetti, Physica C **161**, 598 (1989).
15. J. L. Tallon, R. G. Buckley, P. W. Gilberd, and M. R. Presland, Physica C **158**, 247 (1989).
16. N. Knauf, J. Harnischmacher, R. Müller, R. Borowski, B. Roden, and D. Wohlleben, Physica C **173**, 414 (1991).
17. N. Savvides, Physica C **165**, 371 (1990).
18. J. F. Kwak, E. L. Venturini, and D. S. Ginley, Physica B **148**, 426 (1987).
19. R. L. Peterson and J. W. Ekin, Phys. Rev. B **37**, 9848 (1988).
20. D. Dew-Hughes, Cryogenics **28**, 674 (1988).
21. J. W. Ekin, H. R. Hart, Jr., and A. R. Gaddipati, J. Appl. Phys. **68**, 2285 (1990).
22. F. R. Wang, Q. Z. Wen, C. Y. Li, Y. D. Dai, D. L. Yin, and M. L. Zhou, Modern Phys. Lett. B **2**, 613 (1988).
23. J. W. Ekin, A. I. Braginski, A. J. Panson, M. A. Janocko, D. W. Capone II, N. J. Zaluzec, B. Flandermeyer, O. F. de Lima, M. Hong, J. Kwo, and S. H. Liou, J. Appl. Phys. **62**, 4821 (1987).
24. K. K. Likharev, Rev. Modern Phys. **51**, 101 (1979).
25. S. Martin, A. T. Fiory, R. M. Fleming, G. P. Espinosa, and A. S. Cooper, Appl. Phys. Lett. **54**, 72 (1989).
26. D. P. Hampshire, X. Cai, J. Seuntjens, and D. C. Larbalestier, Supercond. Sci. Technol. **1**, 12 (1988).